# New limits on neutrino electromagnetic interactions and light new physics with XENONnT

Amir N. Khan[*]

*Max-Planck-Institut für Kernphysik, Postfach 103980, D-69029 Heidelberg, Germany*

(Dated: August 17, 2022)

We derive new limits on the neutrino electromagnetic interactions and weakly coupled light vector and scalar mediators using the recent XENONnT data of the solar neutrino-electron elastic scattering. With almost twice the exposure and improved systematics, XENONnT has already reported the world's best constraint on the flavor-independent effective neutrino magnetic moment. We extend this analysis and derive constraints on all the possible electromagnetic interactions and flavor universal light gauge boson couplings and masses which could contribute to the neutrino-electron elastic scattering process. For the electromagnetic interactions, we consider both flavor-independent and flavor-dependent interactions of the neutrino magnetic moments, millicharges, charge radii and anapole moments. The new limits on the magnetic moment, millicharge, vector and scalar interactions are improved by about one order of magnitude, while there is relatively weaker improvement in the case of neutrino charge radii and anapole moments.

## I. INTRODUCTION

The XENONnT experiment has collected new data with a larger detector and total exposure of 1.16 ton-years and with reduced systematic uncertainties and improved background [1]. More importantly, no excess in the range $(1-7)$ keV of the electronic recoil like its predecessor detector XENON1T [2] has been observed. More than 50% background reduction has been achieved in the new upgrade [1]. On one hand, the larger exposure and lower background rate of the experiment increase its sensitivity to dark matter detection, on the other hand, it can also increase its sensitivity to the new physics related to the solar neutrino interactions.

With this motivation in mind, we use the XENONnT new data and derive limits on all possible new interactions related to the massive neutrinos. These include electromagnetic interactions such as neutrino magnetic moment [3–7], neutrino millicharge [8–24], neutrino charge radius [25–28], anapole moment [29–36] and new light vector and scalar mediators that feebly couple to neutrinos and electrons [37–41]. For the electromagnetic interactions, we consider both flavor-independent effective interactions by taking the same couplings for the three neutrino flavors contained in the final solar fluxes and flavor-dependent interactions. In the case of the weakly coupled new light mediators, we only consider the flavor universal and diagonal interactions.

Solar neutrino detectors offer a natural laboratory for testing the flavored new physics models related to the neutrino interactions because of the long baseline. The total flux thus contains all three flavors of neutrinos [42–47]. The total rate is the sum of $\nu_e(\approx 56\%)$, $\nu_\mu(\approx 22\%)$ and $\nu_\tau(\approx 22\%)$ in case of the maximal mixing. In this case, the new physics interaction of muon and tau neutrinos cannot be distinguished. However, in our anal-

ysis here we will assume the non-maximal "23" mixing scheme which makes it possible to distinguish, at least theoretically, between the muon and tau neutrino interactions. This effect has been included in eq. (12). The flavor-dependent constraints become important when one compares the bounds with the flavor-specific experiments [18, 48–50].

After the observation of the recoil electron excess by XENON1T [2], several dark matter candidates and different neutrino nonstandard interactions were used to explain it, while several other studies derived new limits on model-dependent parameters [19, 43, 51–76]. In principle, all those results can be updated with new XENONnT data. However, here we will focus only on the neutrino electromagnetic interactions and the weakly coupled new light mediator that could modify the neutrino-electron elastic scattering at the low energy. We will treat the total predicted background reported by XENONnT by excluding the solar neutrino contribution and then we will calculate the predicted neutrino spectrum in the presence of all the new physics interactions and add them to the background spectrum. We will use this setup to derive the one parameter at-a-time limits and the two parameters allowed parameter spaces.

After setting up the formal structure in section II, we discuss the analysis in section III. In section IV, we present our results and conclude in section V.

## II. FORMALISM

Here we discuss the necessary formalism needed for the calculations of expected rates due to the electromagnetic interactions and for light gauge bosons that mediate in the elastic neutrino-electron scattering process. The electroweak cross-section of the $\nu_\alpha - e$ scattering process in the standard model is given by
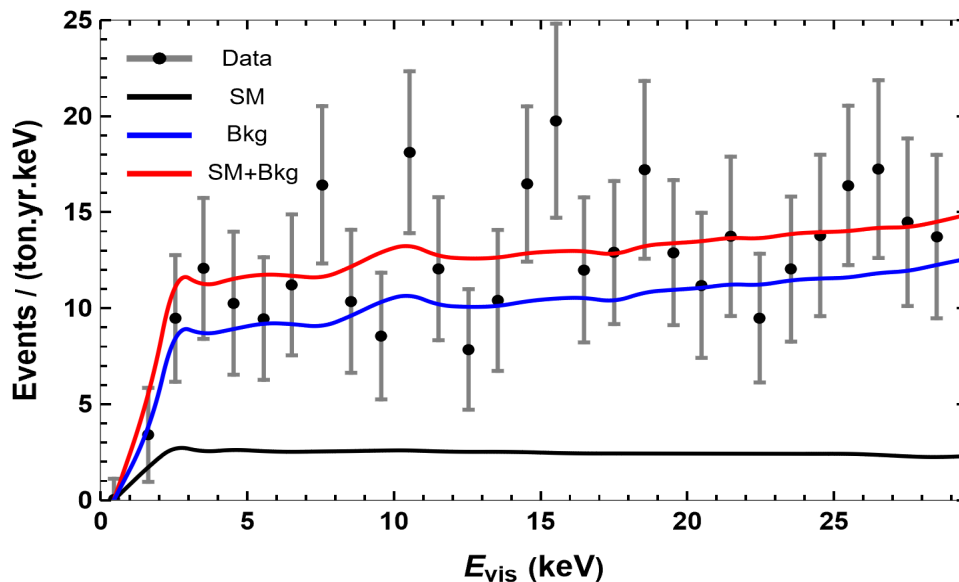
---
[*] amir.khan@mpi-hd.mpg.de

Figure 1.  Data, total background (red), background without solar neutrino contribution (blue) and our prediction for the solar neutrino energy spectrum (black). We obtain the background without the solar neutrino contribution (blue) by subtracting our calculated solar neutrino rates in each energy bin from the total background in the corresponding bin. The data and total background were taken from ref. [1].

$$\left(\frac{d\sigma_{\nu_\alpha e}}{dE_r}\right)_{SM} = \frac{2G_F^2 m_e}{\pi}\left[g_L^2 + g_R^2\left(1-\frac{E_r}{E_\nu}\right)^2 - g_L g_R \frac{m_e E_r}{E_\nu^2}\right], \quad (1)$$

where $G_F$ is Fermi constant, $m_e$ is mass of electron, $g_L = (g_V + g_A)/2 + 1$ for $\nu_e$, $(g_V + g_A)/2$ for $\nu_{\mu,\tau}$, $g_R = (g_V - g_A)/2$ for $\nu_{e,\mu,\tau}$, $g_V = -1/2 + 2\sin^2\theta_W$, $g_A = -1/2$, $E_\nu$ is the incoming neutrino energy and $E_r$ is the electron recoil energy in the detector. We take $\sin^2\theta_W = 0.23867 \pm 0.00016$ in the $\overline{\text{MS}}$ scheme [77] and correct $g_V$ and $g_A$ for the small radiative corrections.

### A.  Electromagnetic Interactions

Among the four types of electromagnetic interactions, only the neutrino magnetic moment cross-section as in the following is added to the standard model cross-section (1) without any interference effects because of the chirality flipping of the neutrinos in the scattering process [3, 5, 78, 79],

$$\left(\frac{d\sigma_{\nu_\alpha e}}{dE_r}\right)_{MM} = \frac{\pi\alpha_{em}^2 \mu_{\nu_\alpha}^2}{m_e^2}\left[\frac{1}{E_r} - \frac{1}{E_\nu}\right], \quad (2)$$

where $\alpha_{em}$ is the electromagnetic fine structure constant and $\mu_{\nu_\alpha}$ is the magnetic moment coupling in units of Bohr magneton $(\mu_B)$. We consider the neutrino flavor conserving cases for all types of electromagnetic interactions. For the millicharge neutrinos, charge radius and

anapole moment, we replace $g_V$ with $\widetilde{g}_V$, where

$$\widetilde{g}_V = g_V + \frac{\sqrt{2}\pi\alpha}{G_F}\left(\frac{\langle r_{\nu_\alpha}^2\rangle}{3} - \frac{a_{\nu_\alpha}}{18} - \frac{q_{\nu_\alpha}}{m_e E_r}\right). \quad (3)$$

Here, $q_{\nu_\alpha}$ is the neutrino fractional electric charge in units of unit charge of electron"e" and $\langle r_{\nu_\alpha}^2\rangle$ and $a_{\nu_\alpha}$ are respectively the neutrino charge radius and anapole moment in units of cm². Notice that among the three quantities neutrino millicharge appears to be more sensitive because of its inverse squared dependence on the electronic recoils. We will discuss this aspect in detail in the following sections.

### B.  Light Mediators

We will derive constraints on the coupling and masses of new light vector and scalar gauge bosons which can contribute to the neutrino-electron elastic scattering process through the general model-independent vector (V), axial-vector (A), scalar (S) and pseudoscalar (P) interactions. At low recoils, due to the fact that the new physics effects are inversely proportional to the recoil electron kinetic energy and due to the better agreement between the expected and observed background, XENONnT data can put stronger or competitive limits on the light mediator couplings and their masses. These interactions are predicted by a wide variety of models [37–41], however, we do not discuss here the possible origin of these interactions. An important aspect of such mediators is that they have low masses and very weak couplings, therefore,

their masses could possibly be generated by spontaneous symmetry breaking well below the electroweak breaking scale. For other phenomenological implications of such interactions, see refs. [80–82].

In the following, we assume additional model independent light Spin-1 ($Z'_\mu$) and spin-0 ($S$) mediators which couple to electrons and to the three flavor of neutrinos with equal coupling strengths via a vector, axial-vector, scalar and pseudoscalar interactions. Such interactions are described by the following Lagrangians:

$$\mathcal{L}_{V'} = -g'_V \left[ \overline{\nu}_L \gamma^\mu \nu_L + \overline{e}\gamma^\mu e \right] Z'_\mu \quad \text{(Vector)}, \tag{4}$$

$$\mathcal{L}_{A'} = -g'_A \left[ \overline{\nu}_L \gamma^\mu \gamma_5 \nu_L + \overline{e}\gamma^\mu \gamma_5 e \right] Z'_\mu \text{ (Axial} - \text{vector)}, \tag{5}$$

$$\mathcal{L}_S = -g_S \left[ \overline{\nu}_R \gamma_5 \nu_L + \overline{e}e \right] S + h.c \quad \text{(Scalar)}, \tag{6}$$

$$\mathcal{L}_P = -g_P \left[ \overline{\nu}_R \gamma_5 \nu_L + i\overline{e}\gamma_5 e \right] S + h.c \text{ (Pseudo} - \text{scalar)}. \tag{7}$$

Here $g'_V, g'_A, g_A$ and $g_P$ are the coupling constants of the corresponding interactions. Since the vector and axial-vector interactions interfere with the standard model interactions, therefore, in the low momentum transfer limit, the standard model couplings with electrons, $g_{V/A}$ in eq. (1) can be replaced by the effective parameters $\widetilde{g}_{V/A}$ [46, 50] as

$$\widetilde{g}_V = g_V + \left( \frac{g^2_{V'}}{\sqrt{2}G_F(2m_e E_r + m^2_{V'})} \right), \tag{8}$$

and

$$\widetilde{g}_A = g_A + \left( \frac{g^2_{A'}}{\sqrt{2}G_F(2m_e E_r + m^2_{A'})} \right), \tag{9}$$

where $g_{V'}$ and $g_{A'}$ are the coupling constants and $m_{V'}$ and $m_{A'}$ are the respective masses of the new vector and axial-vector mediators.

The contribution of scalar mediators is added without interference. In this case, the scalar and pseudo-scalar interaction cross-sections [46, 83] are

$$\left( \frac{d\sigma_{\nu_\alpha e}}{dE_r} \right)_S = \left( \frac{g^4_S}{4\pi(2m_e E_r + m^2_S)^2} \right) \frac{m^2_e E_r}{E^2_\nu}, \tag{10}$$

$$\left( \frac{d\sigma_{\nu_\alpha e}}{dE_r} \right)_P = \left( \frac{g^4_P}{8\pi(2m_e E_r + m^2_P)^2} \right) \frac{m_e E^2_r}{E^2_\nu}, \tag{11}$$

where $g_S$ and $g_P$ are the scalar and pseudoscalar coupling constants and $m_S$ and $m_P$ are, respectively, their masses.

Notice that we do not consider the flavor-dependent light new interactions, although, this is possible with the XENONnT of the solar neutrinos. This is an important direction to pursue because it can be used to test different flavored additional vector type $U(1)'$ models. We leave this for future work.

### C. Expected Energy Spectrum

Next, we define the differential event rates as a function of the visible recoil energy ($E_{vis}$) of electrons to estimate the electromagnetic and the new weak interactions that contribute to the standard model interactions. This can be written as

$$\frac{dN}{dE_{vis}} = N_e \int_{E^{th}_r}^{E^{mx}_r} dE_r \int_{E^{mn}_\nu}^{E^{mx}_\nu} dE_\nu \left( \frac{d\sigma_{\nu_e e}}{dE_r}\overline{P}^m_{ee} + \cos^2\theta_{23}\frac{d\sigma_{\nu_\mu e}}{dE_r}\overline{P}^m_{e\mu} + \sin^2\theta_{23}\frac{d\sigma_{\nu_\tau e}}{dE_r}\overline{P}^m_{e\tau} \right) \frac{d\phi}{dE_\nu}\epsilon(E_{vis})G(E_{vis}, E_r), \tag{12}$$

where $G(E_r, E_{vis})$ is a normalized Gaussian smearing function to account for the detector finite energy resolution with resolution power $\sigma(E_{vis})/E_{vis} = (0.3171/\sqrt{E_{vis}[\text{keV}]}) + 0.0015$ and $\epsilon(E_{vis})$ is the detector efficiency both taken from [1], $d\phi/dE_\nu$ is the solar flux spectra were taken from [84] and $N_e$ is 1.16 ton-year exposure [1]. Here, $d\sigma_{v_\alpha e}/dE_r$ are cross-sections, $\overline{P}^m_{ee}$ and $\overline{P}^m_{e\mu/\tau}$ are the neutrino oscillation length averaged survival ($\nu_e$) and conversion ($\nu_\mu, \nu_\tau$) probabilities of solar neutrinos in the presence of small matter effects as given by,

$$\overline{P}^m_{ee} = s^4_{13} + \frac{1}{2}c^4_{13}(1 + \cos 2\theta^m_{12}\cos 2\theta_{12}) \tag{13}$$

and $\overline{P}^m_{e\mu/\tau} = 1 - \overline{P}^m_{ee}$, where $s_{ij}$, $c_{ij}$ are mixing angles in vacuum and $\theta^m_{12}$ is the matter effects induced

mixing angle which was taken from [77, 85]. We take values of oscillation parameters and their uncertainties from [77] and for the analysis, we consider only the normal ordering scheme. The integration limits are $E^{mn}_\nu = (E_r + \sqrt{2m_e E_r + E^2_r})/2$ and $E^{mx}_\nu$ is the upper limit of each component of the pp-chain and CNO solar neutrinos considered here. We note pp neutrinos are the dominant contributors to energy range of interest here, while the other sources have a negligibly small effect on the energy spectrum due to the lower fluxes. $E^{th}_r = 1$ keV is the detector threshold and $E^{mx}_r = 30$ keV is the maximum electronic recoil energy for the region of interest.

## III. ANALYSIS DETAILS

Having set out all the necessary formulas above, we calculate the differential event rate energy spectrum (eq. 12) as a function of $E_{vis}$ of the solar neutrinos using eqs. (1, 3 and 2) for the standard and for the neutrino electromagnetic interactions and eqs. (1, 8 9, 10 and 11) for the vector and scalar interactions.

We take the total background contribution below 30 keV from ref. [1] and subtract our calculated energy spectrum from the total background. This is shown in blue in fig. 1. Our calculated solar neutrino energy spectrum is shown in black in fig. 1 which agrees well with the solar neutrino spectrum [1]. The main background sources below 30 keV are $^{214}$Pb, $^{85}$Kr, $^{136}$Xe, $^{124}$Xe and materials.

It is important to note that we fit flavor-independent (effective) parameters for all four electromagnetic interactions following the limit reported by XENONnT on the effective magnetic moment. In addition, we derive limits on flavor-dependent parameters since XENONnT, like solar neutrino oscillation experiments, receives fluxes of all the three neutrino flavors. This is clear from eq. (12) where we assume the case of a non-maximal scheme of "23" mixing scheme. For the maximal mixing scheme, the bounds muon and tau flavors would be the same.

To estimate the new physics parameters using XENONnT data we follow the least-squared statistical method and define the following $\chi^2$ function,

$$\chi^2 = \sum_i \left( \frac{(\frac{dN}{dE_{vis}}(1+\alpha) + B)^i_{th} - (\frac{dN}{dE_{vis}})^i_{obs}}{\sigma^i} \right)^2 + \left( \frac{\alpha}{\sigma_\alpha} \right) \tag{14}$$

where the expression in the bracket $(.....)^i_{th}$ corresponds to the expected number of events in the $i-$th bin which is the sum of solar neutrinos rate and the background for each bin, while the bracket $(...)^i_{obs}$ corresponds to the observed number of events and $\sigma^i$ is the experimental uncertainty in the respective bin. The data point with uncertainties and the solar neutrino expected energy rates and the background rates are shown in fig. 1. We add the pull term to account for the theoretical uncertainty which mainly comes from the solar fluxes. We take $\alpha$ as the pull parameter with "$\sigma_\alpha = 10\%$" uncertainty in the fluxes [1]. In addition, we also include penalty terms corresponding to the "$\theta_{12}$" "$\theta_{13}$" and "$\theta_{23}$" oscillation parameters to account for their uncertainties. Using eq. 14, we reproduce the upper limit $\sim 6.26 \times 10^{-12}\mu_B$ at 90% C.L. on the neutrino flavor independent (effective) magnetic moment, as shown in the left-hand side plot of fig. 2, which is in the best agreement with the limit reported in ref. [1], that is, $\sim 6.3 \times 10^{-12}\mu_B$. This result is shown on the left-most in black in fig. 2.

## IV. RESULTS AND DISCUSSION

The results of our analysis for the flavor-dependent neutrino magnetic moments are shown in one-dimensional and two-dimensional contour plots in fig. 2. In both cases, we show the 90% and 99% C.L. allowed regions. In the one-dimensional case, we retain one parameter and put the other two equal to zero while in the two-dimensional case, we fit two parameters and put the third parameter equal to zero. All the 90% C.L. limits are summarized in the first three rows and 2nd column of the table (I). For comparison, we also show bounds from the other experiments in the table.

Next, we repeat the above exercise for the neutrino millicharges, charge radii and neutrino anapole moments. We obtain the one-dimensional and two-dimensional allowed parameter spaces at 90% and 99% C.L., which are shown, respectively, in fig 3, 4 and 5. The bounds at 90% C.L. are summarized in the first three rows and 3rd, 4th and 5th columns of the table (I).

As shown in fig. 2, 3, 4 and 5, we fit both flavor-independent and flavor-dependent parameters for each type of interaction. In the former case, we take the electromagnetic parameter as a common parameter for each of the three neutrino fluxes, while in the latter case we take a separate parameter for each flux corresponding to its flavor. This choice is motivated by the fact that because of the very long baselines, the solar neutrinos contain all three flavors and thus present a natural laboratory for any type of flavor-dependent new physics related to the neutrino interactions. The flavor-independent effective parameter bounds are stronger than the flavor-dependent bounds for all types of interactions because their contributions to the total rate are the same. This is evident from all four figures and from table I. In the case of flavor-dependent interactions, the $\nu_\mu$ and $\nu_\tau$ flavors are distinguished through the atmospheric mixing angle, $\theta_{23}$, as given in eq. 12.

It is interesting to note that among the four types of electromagnetic interactions, the neutrino magnetic moment and millicharge for the flavor-independent and for the $\nu_e$ flavor cases get limits that are stronger by about one order of magnitude than the previous bounds. For the other flavors, there is also a considerable improvement. As compared to the neutrino magnetic moment and milli-charge, the constraints on the charge radii and the neutrino anapole moments have relatively smaller improvement than the previous ones. This is due to the fact that there is no inverse recoil energy dependence in latter cases, as evident from eq. 3.

Next, we fit the couplings and masses of the four types of new weak interactions. All the results in the form of two-dimensional exclusion plots at 90% C.L. are shown in fig. 6, and the corresponding bounds at 90% C.L. are summarized in table (II). From the table, it is clear that there is a significant improvement in limits in all cases. In particular, the vector, axial-vector and scalar coupling limits get stronger by at least one order of magnitude and
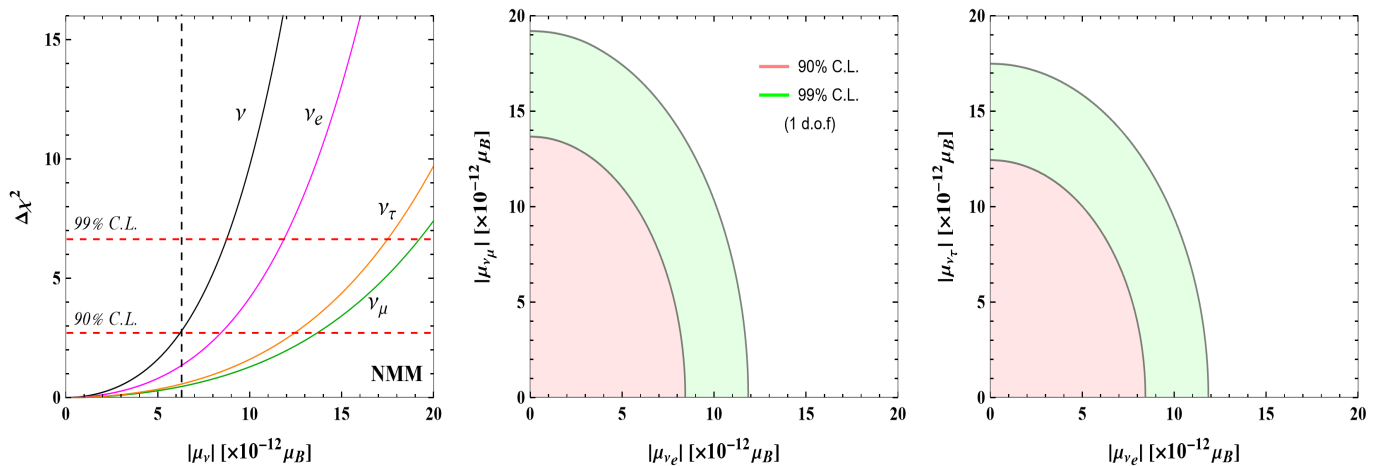
Figure 2. One-dimensional $\Delta\chi^2$ distribution with 90% and 99% C.L. boundaries of neutrino magnetic moments (NMM) and two-dimensional allowed regions at 90% and 99% C.L. with one degree of freedom $\Delta\chi^2$. In the one dimensional case, the distribution in black corresponds to the effective flavor independent magnetic moment.
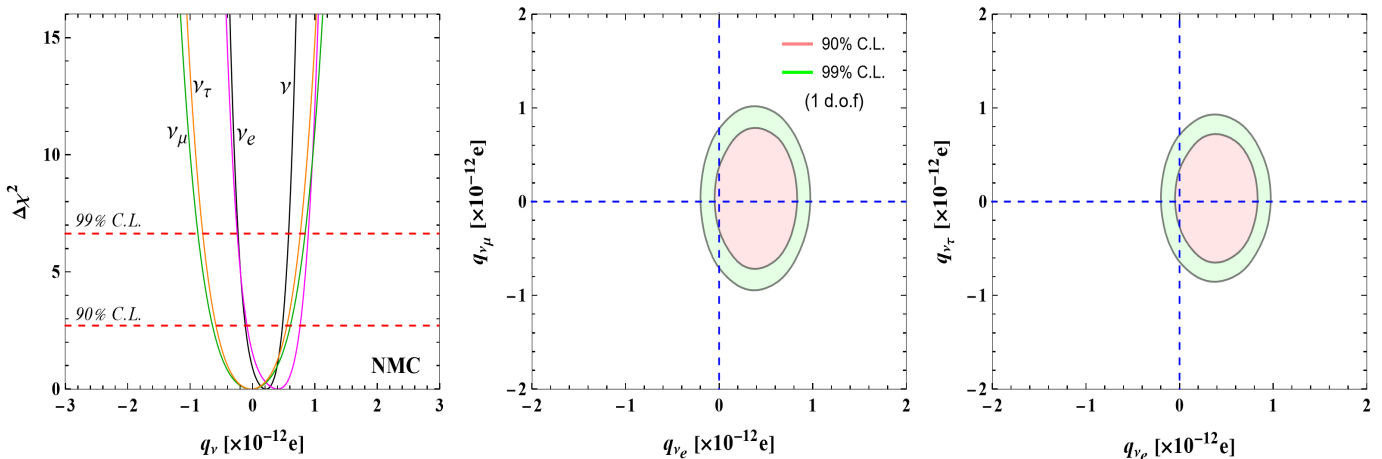


Figure 3. One-dimensional $\Delta\chi^2$ distribution with 90% and 99% C.L. boundaries of neutrino millicharge (NMC) and two-dimensional allowed regions at 90% and 99% C.L. with one degree of freedom $\Delta\chi^2$. In the one-dimensional case, the distribution in black corresponds to the effective flavor- independent neutrino millicharge.

supersede the previous limits from the terrestrial experiments. The vector couplings get the strongest bounds, $g_{V'} \lesssim 1.3$ for the mediator mass of $m_{V'} \lesssim 10$ keV, the axial-vector coupling $g_{A'} \lesssim 1.7$ for the mediator mass of $m_{A'} \lesssim 10$ keV, the scalar coupling $g_S \lesssim 5$ for the mediator mass of $m_S \lesssim 15$ keV and the pseudo-scalar coupling $g_P \lesssim 20$ for the mediator mass of $m_P \lesssim 30$ keV, which are the best constraints so far. Note that these constraints also supersede the bounds from the Panda-XII experiment [46, 91], which is a similar dark matter detector experiment to XENONnT.

## V. SUMMARY AND CONCLUSION

We have analyzed the new data of XENONnT to constrain the electromagnetic interactions and new, feebly coupled, weak interactions. Unlike XENON1T, the new data has not revealed any excess at the low energy electronic recoils, and the experiment has improved its systematics and improved the background. Obviously, with this improvement, stronger constraints from the solar neutrino interactions are expected. With this motivation in mind, we have considered constraining the neutrino magnetic moment, charge radius, millicharge, anapole moment, vector, axial-vector, scalar and pseudoscalar interactions in our analysis. We have first reproduced the 90% C.L. bound on the neutrino the flavor-independent
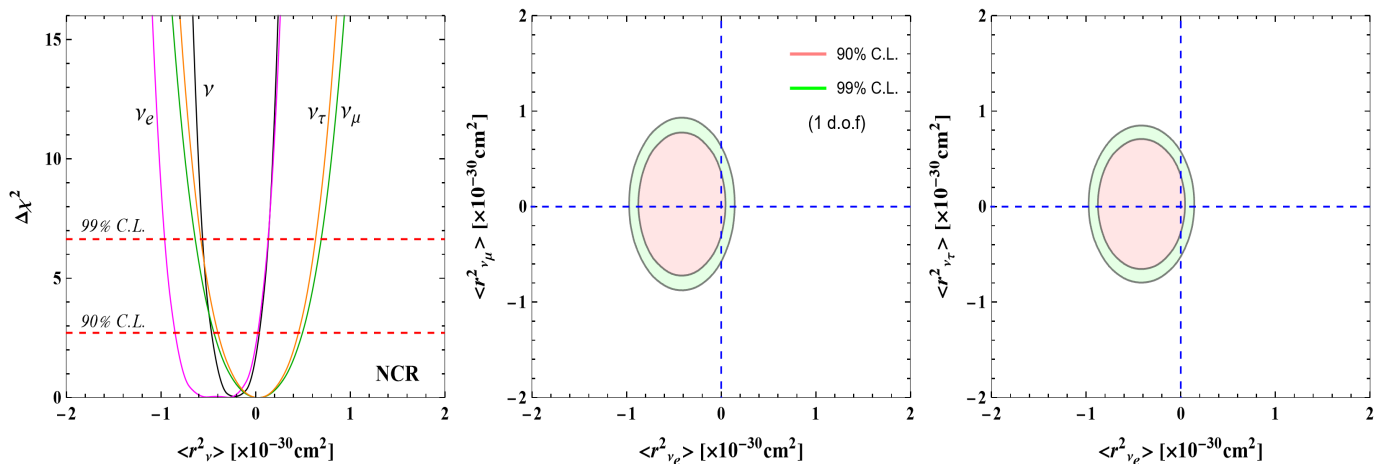
Figure 4. One-dimensional $\Delta\chi^2$ distribution with 90% and 99% C.L. boundaries of neutrino charge radius (NCR) and two-dimensional allowed regions at 90% and 99% C.L. with one degree of freedom $\Delta\chi^2$. In the one dimensional case, the distribution in black corresponds to the effective flavor- independent charge radius.
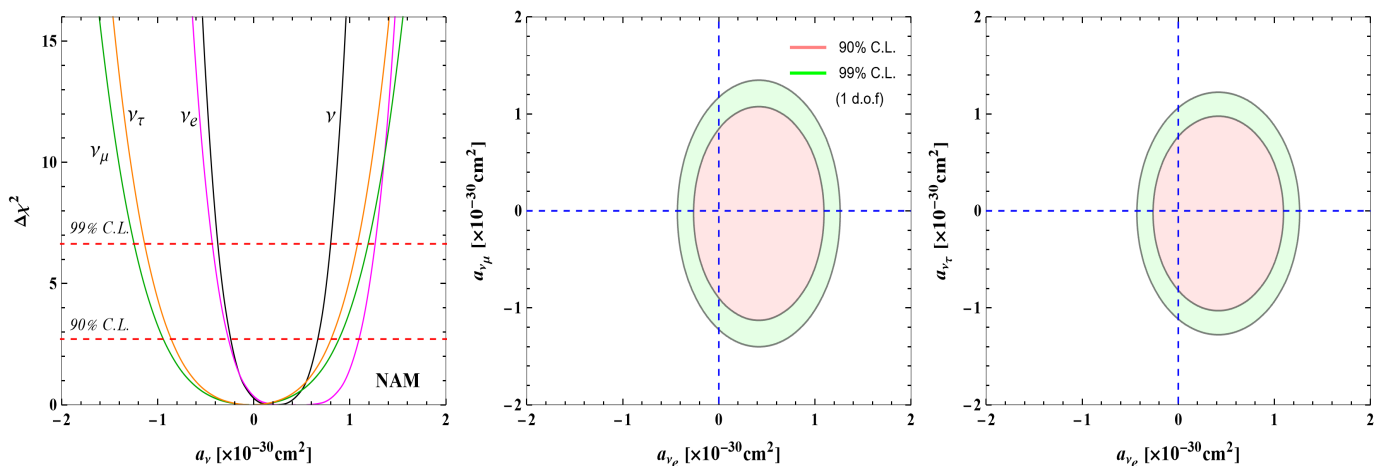


Figure 5. One-dimensional $\Delta\chi^2$ distribution with 90% and 99% C.L. boundaries of neutrino anapole moment (NAM) and two-dimensional allowed regions at 90% and 99% C.L. with one degree of freedom $\Delta\chi^2$. In the one dimensional case, the distribution in black corresponds to the effective flavor- independent anapole moment.

effective neutrino magnetic moment, which agrees well with the one reported by the XENONnT collaboration [1]. To better compare with other laboratory bounds on the flavor-dependent electromagnetic interactions, we have introduced both the effective flavor-independent and flavor-dependent parameters and have constrained them with the new data. All the results are shown in one dimensional $\Delta\chi^2$ distributions and in two-dimensional allowed parameter spaces at 90% and 99% C.L.. The 90 % C.L. limits for all cases are given in table I. For a quick comparison, the bounds from other laboratory experiments and astrophysical observations are also given in the table.

Because of the enhanced sensitivity of the magnetic moment and the neutrino millicharge at lower electronic recoils, we obtain stronger constraints for both cases. The charge radius and anapole moment lack this characteristic and therefore relatively smaller improvement in their bounds can be achieved. The inverse recoil electron energy dependence makes the low energy search data a special probe of the neutrino magnetic moment and neutrino millicharge. The $\nu - e$ scattering constraint on the neutrino magnetic moment and neutrino millicharge are also stronger than those from the coherent elastic neutrino-nucleus scattering [47, 92, 93] for the kinematical reason that the enhanced sensitivity at the lower electronic recoils in the former case is scaled up by the target electron mass, while in the latter case, it is scaled up by the target nuclear mass which partially reduces the enhancement of low energy sensitivity. On the other hand,

| Flavor | $\|\mu_\nu\|[\times 10^{-11}\mu_B]$ | $q_v$ $[\times 10^{-13}e]$ | $\langle r_\nu^2 \rangle$ $[\times 10^{-32}\text{cm}^2]$ | $a_\nu$ $[\times 10^{-32}\text{cm}^2]$ |
|---|---|---|---|---|
| $\nu$ (XENONnT) | $< 0.63$ | $[-1.3,\ 4.7\ ]$ | $[-45,\ 3.0\ ]$ | $[\ -23, 65]$ |
| $\nu_e$ (XENONnT) | $< 0.85$ | $[-2.5,\ 9.0\ ]$ | $[-85,\ 2.0\ ]$ | $[\ -26, 110]$ |
| $\nu_\mu$(XENONnT) | $< 1.37$ | $[-8.9,\ 8.6\ ]$ | $[-45,\ 52\ ]$ | $[-95, 89]$ |
| $\nu_\tau$(XENONnT) | $< 1.24$ | $[7.9,\ 7.8\ ]$ | $[-40,\ 45\ ]$ | $[-86, 79]$ |
| $\nu_e$ (Others) | $\leq 3.9$ (Borexino) <br> $\leq 110$ (LAMPF) <br> $\leq 11$ (Super-K) <br> $\leq 7.4$ (TEXONO) <br> $\leq 2.9$ (GEMMA) | $\leq 15$ <br> (Reactor) | $[0.82,\ 1.27]$ (Solar) <br> $[-5.94,\ 8.28]$ (LSND) <br> $[-4.2,\ 6.6]$ (TEXONO) | $-$ |
| $\nu_\mu$(Others) | $\leq 5.8$ (Borexino) <br> $\leq 68$ (LSND) <br> $\leq 74$ (LAMPF)[7] | $-$ | $[-9,\ 31]$ (Solar) <br> $\leq 1.2$ (CHARM-II) <br> $[-4.2,\ 0.48]$ (TEXONO) | $-$ |
| $\nu_\tau$(Others) | $\leq 5.8$ (Borexino) <br> $\leq 3.9 \times 10^4$ (DONUT) | $\leq 10^{-8}$ <br> (Beam dump) | $[-9,\ 31]$ (Solar) | $-$ |

Table I. 90% C.L. bounds on neutrino magnetic moment, charge radius, millicharge and anapole moment from XENON1T and other laboratory experiments. First row corresponds to the flavor independent effective parameters. For comparison with astrophysical constraints see ref. [86] and for COHERENT see refs. [18]. Apart from Borexino [49] and solar [87], bounds from all other experiments were taken from refs. [49, 86].

| Coupling | XENONnT (**this work**) | PandaX-II | GEMMA | Borexino | TEXONO |
|---|---|---|---|---|---|
| $g_{V'}(\times 10^{-7})$ | $\lesssim 1.3$ | $\lesssim 32$ | $\lesssim 5.0$ | $\lesssim 17$ | $\lesssim 58$ |
| $g_{A'}(\times 10^{-7})$ | $\lesssim 1.7$ | $\lesssim 34$ | $-$ | $-$ | $-$ |
| $g_S\ (\times 10^{-7})$ | $\lesssim 5.0$ | $\lesssim 49$ | $\lesssim 6.0$ | $\lesssim 6.0$ | $-$ |
| $g_P\ (\times 10^{-7})$ | $\lesssim 20$ | $\lesssim 67$ | $-$ | $-$ | $-$ |

Table II. 90% C.L. (2 dof) upper bounds on the coupling constants of four types of interactions considered in this work. These limits correspond to the mediator masses: $m_V' \lesssim 10$ keV (vector), $m_A' \lesssim 10$ keV (axial-vector), $m_S \lesssim 15$ keV (scalar) and $m_P \lesssim 30$ keV (pseudoscalar) interactions. These bounds can also be read directly from fig. 6. The limits for GEMMA [88], Borexino [89], TEXONO [90], PANDA-XII [46] are given for comparison. For comparison with the the astrophysical limits, see ref. [82].

the new limits in the case of neutrino charge radii and neutrino anapole moments are still weaker than previous laboratory constraints.

Comparison with other bounds shows that there is one order of magnitude improvement from other laboratory experiments for the case of magnetic moment and neutrino millicharges, as shown in table I. For the neutrino millicharges, the bound from the neutrality of matter is still eight orders of magnitude stronger than the

new bound. Also, the neutrino millicharge constraints derived in this work are about one order of magnitude weaker than those from the astrophysical observations [21, 22]. However, the future upgrades of XENONnT, LZ, Darkside-20k and DARWIN [94–96] are likely to compete with these constraints or directly detect these interactions.

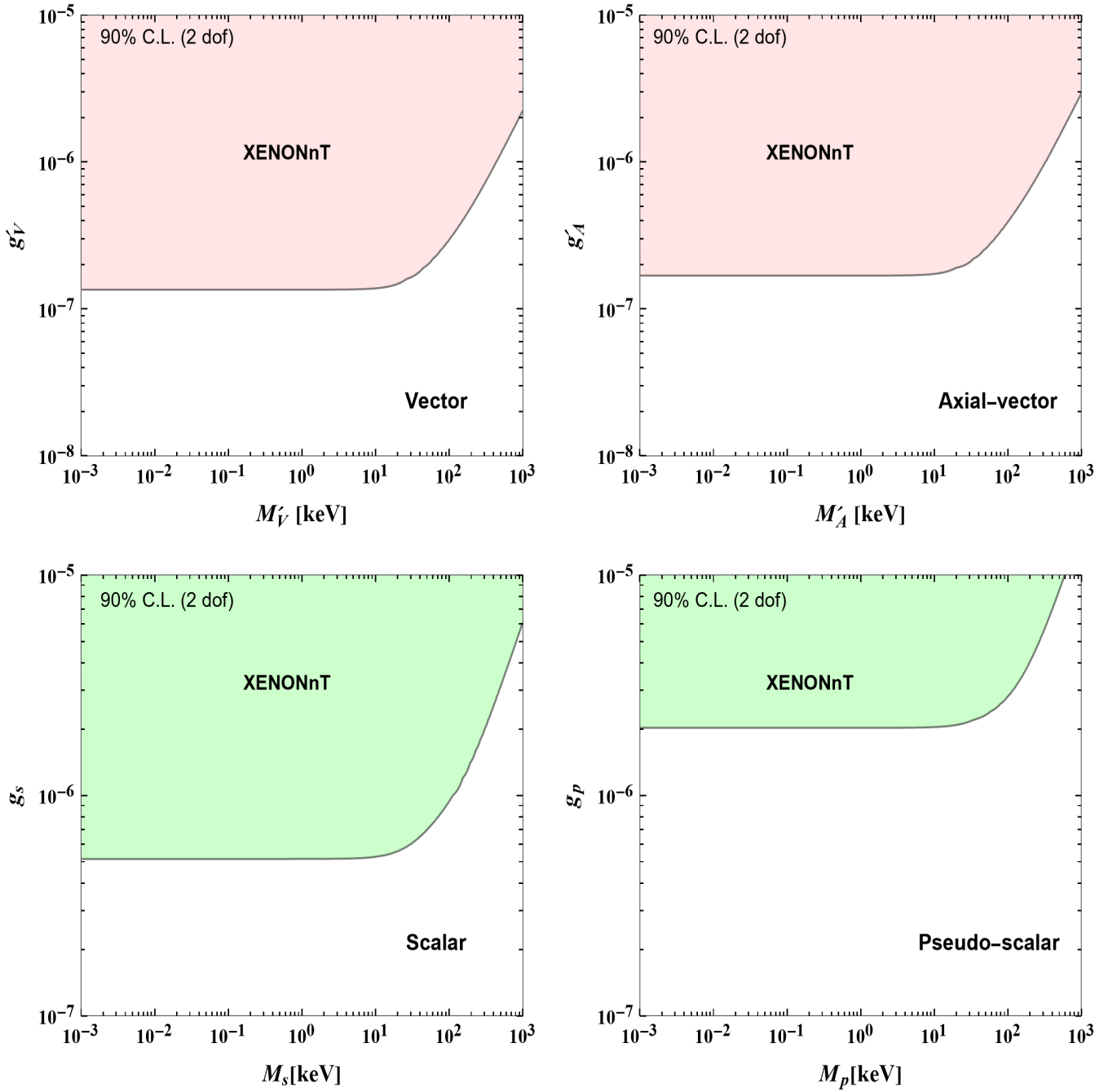In the case of the weakly coupled new light gauge bosons mediating the elastic neutrino-electron scattering

Figure 6. The 90% C.L. two dof $\Delta\chi^2$ excluded regions in the parameter spaces of the light mediator masses and their couplings to neutrinos and electrons using the XENONnT new data.

process, we consider the flavor diagonal and flavor universal interactions. We derive the excluded regions between the respective couplings and masses. The results at 90% C.L. are shown in fig. 6 and all the limits are summarized in table II. Overall, there is one order of magnitude improvement in the limits for the vector coupling in the mediator mass ranges of about 15 keV or below and 30 keV or below for the scalar mediators.

To conclude, neutrino electromagnetic interactions and new weakly coupled vector and scalar interactions are predicted by several models beyond the standard model with massive neutrinos. The observation of tiny yet finite neutrino masses in the oscillation experiments makes such interactions likely in both dedicated neutrino experiments and in the direct detection dark matter experiment like XENONnT through the low energy scattering

processes. Their effects on the astrophysical phenomenon are equally important. The stronger constraints obtained in this work, particularly for the neutrino magnetic moment, neutrino millicharges, and vector and scalar interactions, are an indication of the minimum sensitivity needed to push the bounds further to reveal direct observation of such interactions and rule out or support new physics models.

[1] E. Aprile *et al.*, (2022), arXiv:2207.11330 [hep-ex].
[2] E. Aprile *et al.* (XENON), (2020), arXiv:2006.09721 [hep-ex].
[3] K. Fujikawa and R. Shrock, Phys. Rev. Lett. **45**, 963 (1980).
[4] R. E. Shrock, Nucl. Phys. B **206**, 359 (1982).
[5] P. Vogel and J. Engel, Phys. Rev. D **39**, 3378 (1989).
[6] M. Abak and C. Aydin, Nuovo Cim. A **101**, 597 (1989).
[7] W. Grimus and P. Stockinger, Phys. Rev. D **57**, 1762 (1998), arXiv:hep-ph/9708279.
[8] K. S. Babu and R. N. Mohapatra, Phys. Rev. Lett. **63**, 938 (1989).
[9] K. S. Babu and R. N. Mohapatra, Phys. Rev. D **41**, 271 (1990).
[10] R. Foot, G. C. Joshi, H. Lew, and R. R. Volkas, Mod. Phys. Lett. A **5**, 2721 (1990).
[11] R. Foot, H. Lew, and R. R. Volkas, J. Phys. G **19**, 361 (1993), [Erratum: J.Phys.G 19, 1067 (1993)], arXiv:hep-ph/9209259.
[12] S. Davidson, B. Campbell, and D. C. Bailey, Phys. Rev. D **43**, 2314 (1991).
[13] K. S. Babu, T. M. Gould, and I. Z. Rothstein, Phys. Lett. B **321**, 140 (1994), arXiv:hep-ph/9310349.
[14] G. Bressi, G. Carugno, F. Della Valle, G. Galeazzi, G. Ruoso, and G. Sartori, Phys. Rev. A **83**, 052101 (2011), arXiv:1102.2766 [physics.atom-ph].
[15] S. N. Gninenko, N. V. Krasnikov, and A. Rubbia, Phys. Rev. D **75**, 075014 (2007), arXiv:hep-ph/0612203.
[16] J.-W. Chen, H.-C. Chi, H.-B. Li, C. P. Liu, L. Singh, H. T. Wong, C.-L. Wu, and C.-P. Wu, Phys. Rev. D **90**, 011301 (2014), arXiv:1405.7168 [hep-ph].
[17] L. Singh *et al.* (TEXONO), Phys. Rev. D **99**, 032009 (2019), arXiv:1808.02719 [hep-ph].
[18] A. N. Khan and W. Rodejohann, Phys. Rev. D **100**, 113003 (2019), arXiv:1907.12444 [hep-ph].
[19] A. N. Khan, (2020), arXiv:2006.12887 [hep-ph].
[20] G. Barbiellini and G. Cocconi, Nature **329**, 21 (1987).
[21] G. Raffelt, Phys. Rept. **320**, 319 (1999).
[22] S. Davidson, S. Hannestad, and G. Raffelt, JHEP **05**, 003 (2000), arXiv:hep-ph/0001179.
[23] A. Melchiorri, A. Polosa, and A. Strumia, Phys. Lett. B **650**, 416 (2007), arXiv:hep-ph/0703144.
[24] A. I. Studenikin and I. Tokarev, Nucl. Phys. B **884**, 396 (2014), arXiv:1209.3245 [hep-ph].
[25] J. Bernabeu, L. G. Cabral-Rosetti, J. Papavassiliou, and J. Vidal, Phys. Rev. **D62**, 113012 (2000), arXiv:hep-ph/0008114 [hep-ph].
[26] J. Bernabeu, J. Papavassiliou, and J. Vidal, Phys. Rev. Lett. **89**, 101802 (2002), [Erratum: Phys. Rev. Lett.89,229902(2002)], arXiv:hep-ph/0206015 [hep-ph].
[27] J. Bernabeu, J. Papavassiliou, and J. Vidal, Nucl. Phys.
**B680**, 450 (2004), arXiv:hep-ph/0210055 [hep-ph].
[28] K. Fujikawa and R. Shrock, Phys. Rev. D **69**, 013007 (2004), arXiv:hep-ph/0309329.
[29] Y. B. Zel'dovich, Soviet Phys. JETP **6**, 1184 (1958).
[30] Y. B. Zel'dovich and A. Perelomov, Zhur. Eksptl'. i Teoret Fiz. **39** (1960).
[31] A. Barroso, F. Boudjema, J. Cole, and N. Dombey, Z. Phys. C **28**, 149 (1985).
[32] M. Abak and C. Aydin, Europhys. Lett. **4**, 881 (1987).
[33] M. Musolf and B. R. Holstein, Phys. Rev. D **43**, 2956 (1991).
[34] V. M. Dubovik and V. E. Kuznetsov, Int. J. Mod. Phys. A **13**, 5257 (1998), arXiv:hep-ph/9606258.
[35] A. Rosado, Phys. Rev. **D61**, 013001 (2000).
[36] H. Novales-Sanchez, A. Rosado, V. Santiago-Olan, and J. J. Toscano, AIP Conf. Proc. **1540**, 21 (2013).
[37] P. Fayet, Phys. Lett. B **69**, 489 (1977).
[38] C. Boehm, Phys. Rev. D **70**, 055007 (2004), arXiv:hep-ph/0405240.
[39] P. Langacker, Rev. Mod. Phys. **81**, 1199 (2009), arXiv:0801.1345 [hep-ph].
[40] E. A. Paschos, (2021), arXiv:2110.01004 [hep-ph].
[41] P. Fayet, Phys. Rev. D **103**, 035034 (2021), arXiv:2010.04673 [hep-ph].
[42] A. N. Khan and D. W. McKay, JHEP **07**, 143 (2017), arXiv:1704.06222 [hep-ph].
[43] d. Amaral, Dorian Warren Praia, D. G. Cerdeno, P. Foldenauer, and E. Reid, (2020), arXiv:2006.11225 [hep-ph].
[44] P. Coloma, M. C. Gonzalez-Garcia, and M. Maltoni, JHEP **01**, 114 (2021), arXiv:2009.14220 [hep-ph].
[45] A. M. Suliga, S. Shalgar, and G. M. Fuller, JCAP **07**, 042 (2021), arXiv:2012.11620 [astro-ph.HE].
[46] A. N. Khan, Phys. Lett. B **819**, 136415 (2021), arXiv:2008.10279 [hep-ph].
[47] A. N. Khan, (2022), arXiv:2203.08892 [hep-ph].
[48] M. Deniz *et al.* (TEXONO), Phys. Rev. D **81**, 072001 (2010), arXiv:0911.1597 [hep-ex].
[49] M. Agostini *et al.* (Borexino), Phys. Rev. D **96**, 091103 (2017), arXiv:1707.09355 [hep-ex].
[50] M. Lindner, F. S. Queiroz, W. Rodejohann, and X.-J. Xu, JHEP **05**, 098 (2018), arXiv:1803.00060 [hep-ph].
[51] C. Boehm, D. G. Cerdeno, M. Fairbairn, P. A. Machado, and A. C. Vincent, (2020), arXiv:2006.11250 [hep-ph].
[52] D. Aristizabal Sierra, V. De Romeri, L. Flores, and D. Papoulias, (2020), arXiv:2006.12457 [hep-ph].
[53] N. Okada, S. Okada, D. Raut, and Q. Shafi, (2020), arXiv:2007.02898 [hep-ph].
[54] M. Lindner, Y. Mambrini, T. B. de Melo, and F. S. Queiroz, (2020), arXiv:2006.14590 [hep-ph].
[55] G. Alonso-Álvarez, F. Ertas, J. Jaeckel, F. Kahlhoefer, and L. Thormaehlen, (2020), arXiv:2006.11243 [hep-ph].

[56] M. Chala and A. Titov, (2020), arXiv:2006.14596 [hep-ph].

[57] S.-F. Ge, P. Pasquini, and J. Sheng, (2020), arXiv:2006.16069 [hep-ph].

[58] K. Benakli, C. Branchina, and G. Lafforgue-Marmet, (2020), arXiv:2007.02655 [hep-ph].

[59] S. Chigusa, M. Endo, and K. Kohri, (2020), arXiv:2007.01663 [hep-ph].

[60] T. Li, (2020), arXiv:2007.00874 [hep-ph].

[61] S. Baek, J. Kim, and P. Ko, (2020), arXiv:2006.16876 [hep-ph].

[62] Y. Gao and T. Li, (2020), arXiv:2006.16192 [hep-ph].

[63] P. Ko and Y. Tang, (2020), arXiv:2006.15822 [hep-ph].

[64] H. An and D. Yang, (2020), arXiv:2006.15672 [hep-ph].

[65] D. McKeen, M. Pospelov, and N. Raj, (2020), arXiv:2006.15140 [hep-ph].

[66] I. M. Bloch, A. Caputo, R. Essig, D. Redigolo, M. Sholapurkar, and T. Volansky, (2020), arXiv:2006.14521 [hep-ph].

[67] R. Budnik, H. Kim, O. Matsedonskyi, G. Perez, and Y. Soreq, (2020), arXiv:2006.14568 [hep-ph].

[68] Y. Farzan and M. Rajaee, (2020), arXiv:2007.14421 [hep-ph].

[69] V. Khruschov, (2020), arXiv:2008.03150 [hep-ph].

[70] J. Kim, T. Nomura, and H. Okada, (2020), arXiv:2007.09894 [hep-ph].

[71] A. Bally, S. Jana, and A. Trautner, (2020), arXiv:2006.11919 [hep-ph].

[72] G. Arcadi, A. Bally, F. Goertz, K. Tame-Narvaez, V. Tenorth, and S. Vogl, (2020), arXiv:2007.08500 [hep-ph].

[73] I. M. Shoemaker, Y.-D. Tsai, and J. Wyenberg, (2020), arXiv:2007.05513 [hep-ph].

[74] S. Shakeri, F. Hajkarim, and S.-S. Xue, (2020), arXiv:2008.05029 [hep-ph].

[75] F. Takahashi, M. Yamada, and W. Yin, (2020), arXiv:2006.10035 [hep-ph].

[76] F. Takahashi, M. Yamada, and W. Yin, (2020), arXiv:2007.10311 [hep-ph].

[77] P. A. Zyla *et al.* (Particle Data Group), PTEP **2020**, 083C01 (2020).

[78] M. Dvornikov and A. Studenikin, Phys. Rev. D **69**, 073001 (2004), arXiv:hep-ph/0305206.

[79] M. S. Dvornikov and A. I. Studenikin, J. Exp. Theor. Phys. **99**, 254 (2004), arXiv:hep-ph/0411085.

[80] M. Pospelov, Phys. Rev. D **84**, 085008 (2011), arXiv:1103.3261 [hep-ph].

[81] M. Pospelov and J. Pradler, Phys. Rev. D **85**, 113016 (2012), [Erratum: Phys.Rev.D 88, 039904 (2013)], arXiv:1203.0545 [hep-ph].

[82] R. Harnik, J. Kopp, and P. A. Machado, JCAP **07**, 026 (2012), arXiv:1202.6073 [hep-ph].

[83] D. G. Cerdeño, M. Fairbairn, T. Jubb, P. A. N. Machado, A. C. Vincent, and C. Bœhm, JHEP **05**, 118 (2016), [Erratum: JHEP 09, 048 (2016)], arXiv:1604.01025 [hep-ph].

[84] J. N. Bahcall and C. Pena-Garay, New J. Phys. **6**, 63 (2004), arXiv:hep-ph/0404061.

[85] I. Lopes and S. Turck-Chièze, Astrophys. J. **765**, 14 (2013), arXiv:1302.2791 [astro-ph.SR].

[86] C. Giunti, K. A. Kouzakov, Y.-F. Li, A. V. Lokhov, A. I. Studenikin, and S. Zhou, Annalen Phys. **528**, 198 (2016), arXiv:1506.05387 [hep-ph].

[87] A. N. Khan, J. Phys. G **46**, 035005 (2019), arXiv:1709.02930 [hep-ph].

[88] A. G. Beda, E. V. Demidova, A. S. Starostin, V. B. Brudanin, V. G. Egorov, D. V. Medvedev, M. V. Shirchenko, and T. Vylov, Phys. Part. Nucl. Lett. **7**, 406 (2010), arXiv:0906.1926 [hep-ex].

[89] M. Agostini *et al.* (BOREXINO), Nature **562**, 505 (2018).

[90] M. Deniz *et al.* (TEXONO), Phys. Rev. D **82**, 033004 (2010), arXiv:1006.1947 [hep-ph].

[91] X. Zhou *et al.* (PandaX-II), (2020), arXiv:2008.06485 [hep-ex].

[92] A. N. Khan, (2022), arXiv:2201.10578 [hep-ph].

[93] P. Coloma, M. C. Gonzalez-Garcia, M. Maltoni, J. a. P. Pinheiro, and S. Urrea, JHEP **07**, 138 (2022), arXiv:2204.03011 [hep-ph].

[94] J. Aalbers *et al.* (DARWIN), (2020), arXiv:2006.03114 [physics.ins-det].

[95] C. Aalseth *et al.*, Eur. Phys. J. Plus **133**, 131 (2018), arXiv:1707.08145 [physics.ins-det].

[96] J. Aalbers *et al.* (DARWIN), JCAP **11**, 017 (2016), arXiv:1606.07001 [astro-ph.IM].